

Trends, Physical Causes, and Attribution of the North American Winter Temperature Dipole

Deepti Singh¹, Daniel L. Swain¹, Justin S. Mankin¹, Daniel E. Horton^{1,2}, Leif Thomas¹,
and Noah S. Diffenbaugh^{1,2}

¹ Department of Earth System Science, Stanford University, Stanford, CA, USA

² Woods Institute for the Environment, Stanford University, Stanford, CA, USA

8

9

10 * corresponding author:

11

12 Deepti Singh

13 singhd@stanford.edu

14 473 Via Ortega

15 Stanford, CA, 94305-4216

16 USA

17 650-468-8791

18

19

21 **Abstract:**

22

23 **1. Introduction**

24 Recent winters in North America, particularly 2013-2014 and 2014-2015, have been
25 characterized by a number of high-impact meteorological events that have had substantial
26 agricultural, hydrological, economic and humanitarian impacts [NCDC ref]. Parts of the
27 western United States have experienced exceptionally warm conditions that have
28 aggravated the ongoing extraordinary multi-year drought¹. These unusually warm
29 temperatures have been accompanied by record low snowpack, early snowmelt and
30 increased wildfire risk that have adversely affected agricultural activities, ecosystems,
31 and water availability in the West [ref]. Simultaneously, the central and eastern U.S. have
32 experienced frequent cold air outbreaks and extreme winter storms that have crippled
33 major cities and caused billions of dollars in economic losses [ref].

34

35 These spatially disparate events are linked by a persistent, highly amplified atmospheric
36 pattern that extends over North America and the adjacent north Pacific and north Atlantic
37 basins [ref]. Characterized by an anomalous mid-tropospheric ridge extending over
38 western North America, Alaska and the Arctic², and a downstream trough over the
39 central and northeastern U.S., this pattern represents an amplification of the winter jet
40 stream climatological state. During recent winters, the anomalous western ridge has
41 resulted in a more meridional path of the jet stream over the region³, displacing the storm
42 tracks northwards in the west and facilitating cold Arctic air downstream into the region
43 east of the Rockies.

44

45 Several mechanistic hypotheses have been posed in the literature regarding the causes of
46 the atmospheric configuration associated with the occurrence of these winter surface
47 temperature extremes. These primarily include the effect of late-summer polar sea-ice
48 loss and Arctic Amplification on the mid-latitude jet stream wave pattern^{4–6}, enhanced
49 autumn Eurasian snow cover^{7–9}, and variability of the tropical Pacific sea surface
50 temperatures^{10–14}. Extensive sea-ice loss accompanying rapid relative warming of the
51 Arctic, can influence the mid-latitude planetary waves through an enhancement of the
52 vertical heat and moisture fluxes into the atmosphere^{15–17}, the barotropic-baroclinic
53 interactions between the high- and mid-latitudes in the following winter^{9,18}, and a
54 modification of the poleward temperature gradient that affects the strength and amplitude
55 of the jet stream^{5,19}. Enhanced Eurasian snow extent in October can result in a negative
56 Arctic Oscillation-like response in the northern hemisphere wintertime circulation
57 through a series of stratospheric-tropospheric interactions^{7,9,20}. These two mechanisms are
58 potentially linked since the Eurasian snow cover advance and extent in October is related
59 to the increased advection of moisture associated with tropospheric warming in the
60 Arctic, and sea-ice loss in the Barents and Kara Seas in Autumn^{4,8,17,21,22}. The third
61 mechanism involves an enhancement of ridging in the NE Pacific and western U.S. due
62 to the poleward propagation of quasi-stationary Rossby waves that originate in the region
63 of tropospheric heating anomalies in the tropical Pacific^{10–12}.

64

65 The above hypotheses suggest linkages of these forcings to the seasonal-scale circulation
66 patterns. However, these meteorological events, occurring on multiple timescales,

67 represent an interplay between the seasonal circulation and daily-scale transient
68 processes. Although individual daily-scale events can have substantial impact, few
69 studies have examined the processes leading up to their occurrence. Further, previous
70 studies have focused either on the ridge in the west^{2,10,11} or the extreme cold events in the
71 east^{8,9,17,23}. Since these events are related by the driving physical mechanism and
72 topographical factors, we investigate the “dipole” of co-occurring warm extremes in the
73 west and cold extremes in the east termed as the North American Winter Temperature
74 Dipole (NAWTD) that has been particularly noticeable in recent winter seasons.

75

76 This study is motivated by the need to better characterize the causes of the specific,
77 atmospheric and surface configurations that have been associated with substantial social
78 and environmental impacts over North America. We develop metrics that capture the
79 dipole character of these co-occurring temperature extremes and examine the atmospheric
80 precursors to these events on daily to monthly timescales to investigate the existence of
81 tropical, mid-latitude and high-latitude forcing mechanisms. We quantify long-term
82 trends in these surface temperature metrics, and relate the trends to changes in the
83 temporal characteristics of mid-tropospheric circulation patterns across North America.
84 Lastly, we address the question of whether the observed trends in the dipole events are
85 attributable to climate forcings or “natural” climate variability.

86

87 **2. Materials and Methods**

88 ***2.1 Data Sources***

89 We use historical (2-meter) daily maximum and minimum temperatures, geopotential
90 height and omega fields from NCEP/NCAR -Reanalysis 1 data
91 (<http://www.esrl.noaa.gov/psd/>) for the satellite era (1980-present) at 2.5 degree
92 resolution. Further, we also use daily maximum and minimum temperature fields from
93 the Oregon State University's PRISM Climate Group
94 (<http://www.prism.oregonstate.edu/>), which are available from 1981-present at a 4 km
95 resolution. We analyze the winter season temperatures from these datasets, defined as
96 December, January and February. We note here that the latest winter season from the
97 PRISM dataset is based on preliminary data.

98

99 To examine the effect of historical forcing on the likelihood of the observed trends, we
100 analyze NCAR's Large Ensemble climate modeling experiment ("LENS"). The multi-
101 member ensemble is designed to simulate internal (or natural) variability that is intrinsic
102 to the climate system by running many realizations of a single model, with the
103 realizations differing only in slight perturbations of the initial conditions²⁴. LENS was
104 run with the CESM1 coupled global climate model, with ~1-degree horizontal resolution
105 in the atmospheric component (CAM5). At the time of acquisition, 35 ensemble members
106 were available for 1920-2005 in the historical experiment (HIST), and 1800 years were
107 available for the single-realization pre-industrial control (PIcontrol). The 35 realizations
108 of the historical simulations have identical radiative forcing but are initialized with
109 slightly different atmospheric conditions. The PIcontrol simulations provide an
110 opportunity to examine the internal variability in a climate that is unaffected by external
111 forcings.

112

113 ***2.2 Clustering of Atmospheric Circulation Patterns***

114 We use the Self-Organizing Maps (SOM)^{25–27} methodology to perform an unsupervised
115 clustering of winter atmospheric patterns for the 1980–2014 period over the domain 20–
116 80°N and 150–340°E. SOMs use a neural network-based cluster analysis technique that
117 uses an iterative procedure to categorize high dimensional data into a pre-defined number
118 of topologically-ordered representative clusters or nodes²⁵. We apply this methodology to
119 daily 500mb geopotential height anomaly fields from the NCEP/NCAR Reanalysis
120 dataset. Anomalies are calculated by removing the seasonal-cycle (climatological daily
121 mean) at each grid point. The categorization of these daily atmospheric patterns is based
122 on minimizing the Euclidean distance between iteratively updated nodes and the daily
123 geopotential height anomalies. Unsupervised clustering implies that no prior knowledge
124 of the types of circulation patterns is required.

125

126 Although previous studies [ref] have proposed different criteria for selecting the number
127 of nodes for clustering based on the significance of the patterns^{26,28,29}, there is no
128 universally accepted method for this selection^{27,30}. The suitability of the number of nodes
129 varies depending on the application, and is a balance between the distinctiveness of the
130 nodes and their significance³⁰. Rare atmospheric patterns are unlikely to be captured with
131 a small number of nodes, whereas a large number of nodes can result in substantial
132 similarity between patterns³¹. We perform our analysis with a 20-node (4 by 5) SOM,
133 which we find is sufficient to qualitatively capture the atmospheric pattern associated
134 with dipole events without substantial similarity between adjacent patterns. Following

135 Horton et al.³⁰, we test the sensitivity of our results using fewer and greater number of
136 nodes (in our case 4, 8, and 35 nodes).

137

138 Since we examine changes in the temporal characteristics of these nodes, there is a
139 concern that uniform thermal expansion of the troposphere caused by recent warming
140 could create spurious trends in these characteristics. Some previous studies have therefore
141 removed the local or domain-averaged trend^{32,33} in geopotential heights from each grid
142 point to account for this effect. However, it has been more recently shown that
143 geopotential heights display spatially heterogeneous trends in recent decades associated
144 with changes in the large-scale dynamics and thermal dilation, and that the latter does not
145 substantially alter the magnitude or direction of the trends in daily-scale atmospheric
146 circulation patterns during this short observational period²⁷. For these reasons, we have
147 chosen not to remove the local or regional trend in geopotential heights for this time
148 period.

149

150 ***2.3 Temperature Extremes***

151 Daily temperature extremes are calculated based on a percentile threshold of their
152 distribution in the baseline period (defined as 1980-2000). The threshold for warm and
153 cold extremes is defined as the 84th percentile of the winter (DJF) daily maximum and
154 15th percentile of the winter daily minimum temperature distributions in the baseline at
155 each grid point. Extreme events are defined as exceedances of the daily maximum in the
156 west and minimum temperatures in the east (>84th percentile for warm extremes and
157 <15th percentile for cold extremes) of these thresholds at each grid point. We de-trend the

158 time series of daily maximum and minimum temperatures before calculating the
159 respective temperature thresholds.

160

161 For the purpose of defining a metric to describe the warm-west/cool-east surface
162 temperature anomaly pattern, we divide the U.S. into two domains approximately
163 separated by the eastern edge of the Rockies – west (25-50°N, 130-103°W) and east (25-
164 50°N, 103-65°W). We define a surface dipole event (NAWTD) as a day with
165 simultaneously occurring warm extremes (daily maximum temperatures > 84th percentile)
166 in the west and cold extremes (daily minimum temperatures < 15th percentile) in the east
167 over at least x% of the land grid points within each domain. We examine dipole events
168 with increasing spatial coverage by varying the area threshold (x) from 5% to 30%. We
169 restrict our analysis to 30% of the area to avoid getting many years of the already small
170 observational record with no dipole events. By definition, events based on a higher area
171 fraction are subsets of the dipole events with smaller fraction of the land grid points
172 experiencing extremes.

173

174 ***2.4 Quantification of trends***

175 Using a methodology similar to that used in Horton et al.²⁷ and Cassano et al.³⁴, we
176 partition the observed trends in event occurrence between different atmospheric patterns
177 using the following formulation:

$$E = \sum_p f_p n_{ep} = \sum_p (\bar{f}_p + f'_p) (\bar{n}_{ep} + n'_{ep})$$

178 where f_p is the frequency of occurrence of a SOM pattern p in a given season and n_{ep} is
179 the number of events associated with the occurrence of each SOM. These variables are

180 further represented by their time mean (\bar{f}_p and \bar{n}_{ep}) and deviation (f'_p and n'_{ep}) from the
181 time mean. Therefore, the temporal trend in the events ($\frac{\partial E}{\partial t}$) can be related to these
182 quantities as follows:

$$183 \quad \frac{\partial E}{\partial t} = \sum_p \frac{\partial f'_p}{\partial t} * \bar{n}_{ep} + \sum_p \frac{\partial n'_{ep}}{\partial t} * \bar{f}_p + \sum_p \partial \frac{n'_{ep} * f_p}{\partial t}$$

184 The terms on the right side of the equation represent the contributions of trends in the
185 frequency of occurrence of a SOM pattern p , trends in the number of events associated
186 with each pattern, and the contribution from the covariance of these variables (i.e
187 interaction term).

188 ***2.5 Attribution of trends***

189 We use the single model, multi-ensemble member LENS ensemble that is designed to
190 simulate the natural variability of the climate system.
191 Using the LENS ensemble, we investigate the likelihood of the observed positive trend in
192 the frequency and intensity of the dipole characteristics in the historical and pre-industrial
193 climate. We generate a distribution of 38-year trends for the historical climate (1968-
194 2005) from the 35 realizations in the historical forcing simulations (HIST) and for the
195 pre-industrial climate using non-overlapping periods from the ~1800 year control
196 simulation (PIcontrol) of the LENS ensemble. The PIcontrol distribution represents the
197 range of trends from natural variability alone whereas the HIST distribution represents
198 the range of natural variability superimposed on the response of the climate system to
199 external forcings.

200

201 ***2.5 Statistical Significance Testing***

202 In this analysis, we estimate trends in the frequency of event occurrence, the frequency of
203 pattern occurrence, and the fraction of events associated with each SOM pattern in each
204 winter season. Since the assumption of normality (which is a prerequisite for a linear
205 regression model) is not met by these characteristics, we use a non-parametric
206 bootstrapping approach to estimate trends and their significance using linear least squares
207 regression. We bootstrap the residuals of the linear regression to calculate bootstrapped
208 estimates of the regression coefficients. Further, bootstrapping also provides a more
209 accurate estimate of the trend coefficients when the underlying sample size is small. We
210 also test for temporal autocorrelation and do not find any significant correlation in these
211 time series (*Will show in supplement as Noah suggested*).

212

213 **3. Characterizing the North American Winter Temperature Dipole (NAWTD) and**
214 **its associated circulation pattern**

215 During recent winters of 2013-2014 and 2014-2015, North America has witnessed a
216 pattern of anomalously warm temperatures in the west and concurrent anomalously cool
217 temperatures in the east^{11,14}. On a seasonal-scale, the 2014-2015 winter was the warmest
218 in the western U.S. since 1980 with an unprecedented fraction (~40%) of the domain
219 experiencing daily maximum temperature exceeding their winter warm thresholds (Fig.
220 1 a,b; red lines). Similarly, the 2013-2014 winter was the coolest in the eastern U.S. since
221 1980 with a record fraction of the domain (~28%) experiencing daily minimum
222 temperatures below their winter cold thresholds (Fig. 1a,b; blue lines). Consequently, the
223 difference in spatially averaged land surface winter season temperatures in the western

224 and eastern U.S. had an unprecedented magnitude during both these seasons (Fig. 1a,
225 black line).

226

227 This dipole in winter surface temperatures is accompanied by an east-west circulation
228 dipole in the mid-troposphere that has received considerable scientific attention in the
229 literature^{10,2,11}. This seasonal-scale, persistent circulation dipole refers to the pattern of a
230 strengthened ridge over the Gulf of Alaska and western North America, and a deepened
231 trough over central-eastern North America that allows frequent cold air outbreaks from
232 the Arctic. Combined with other meteorological features, the topography of the western
233 U.S. influences the location of the climatological wave pattern in the mid-troposphere,
234 deflecting the jet stream northward over the western U.S. and southward east of the
235 Rocky Mountains. Even though the circulation dipole is a feature that persisted on a
236 seasonal-scale during winter 2013-2014 and 2014-2015, the surface temperature extremes
237 are a daily-scale phenomenon. The Rockies also serve as an approximate division in the
238 recently observed winter surface temperature anomalies, creating the warm-west/cool-
239 east dipole pattern.

240

241 Here, we characterize the simultaneous occurrence of daily-scale surface temperature
242 extremes of opposite signs in the west and east by defining a metric that encompasses the
243 spatial extent of the dipole pattern and the temporal variability of the spatial pattern, and
244 is informed by the driving physical mechanism (Methods). Figure 1c shows the
245 composite temperature anomalies across the U.S. domain for NATWD events defined

246 with 15% of the western and eastern domains exhibiting warm or cold extremes. A
247 majority of these events occur later in the season in January (37%) and February (40%).
248 These events are associated (Fig. 1d) with a coherent large-scale circulation with an
249 amplified wave-like feature extending from the North Pacific to the North Atlantic in the
250 mid-troposphere (500mb). Though this pattern is primarily restricted to the mid-latitudes
251 with an anomalous ridge over the western U.S. and an anomalous trough over the eastern
252 U.S, substantial positive anomalies extend from the western U.S. extend over to the
253 Arctic.

254

255 **4. Links to the remote forcings**

256 Several hypothesized mechanisms link the occurrence of such events to sea-ice loss in the
257 Arctic^{2,5,6,31}, increased snow cover over the Eurasian continent^{4,9}, and sea surface
258 temperatures in the Pacific^{11,14,10}. These mechanisms operate on seasonal to interannual
259 timescales and are likely to influence the seasonal mean state of the jet stream and the
260 climatological ridge-trough pattern over North America. Through an analysis of
261 atmospheric circulation patterns, we investigate similar remote linkages of the
262 atmospheric pattern associated with the dipole events, acting on weekly to monthly
263 timescales. We propose that these events result from sub-seasonal scale processes
264 embedded within the context of the seasonal circulation that might be modulated through
265 these remote-forcing mechanisms.

266

267 Focusing on dipole events that have a medium spatial extent (15% fractional area
268 threshold), we analyze the composite lead-lag relationships in 500mb geopotential height

269 anomalies and vertical velocities (Fig. 2). The existence of substantial anomalies over the
270 northern hemisphere mid- and high latitudes preceding these events indicates the role of
271 remote forcings (Fig. 2a). Weak ridging over western North America and a positive
272 North Atlantic Oscillation (NAO) like pattern exists 30 days prior to the occurrence of
273 these dipole events. Persistence of the ridge for at least 30 days indicates the existence of
274 a seasonal-scale anomaly over the region. This strengthening of the Icelandic Low is
275 followed by the development of anomalously low geopotential heights over the Barents
276 Sea and northwestern Eurasia setting up a north-south dipole over the east Atlantic and
277 western Eurasia (at lag = 20 days) that strengthens and shifts eastward. This pattern is
278 conducive to the occurrence of more frequent cold air outbreaks over central and east
279 Asia^{4,6}. The north-south dipole strengthens the meridional geopotential height gradient,
280 subsequently strengthening the jet-level winds downstream in the East Asia jet exit
281 region. Following the eastward shift of this geopotential height dipole, a cyclonic
282 circulation develops in the central Pacific 10 days prior to the event. This low deepens in
283 subsequent days, concurrent with the amplification of large positive anomalies in the
284 region to the north in the Arctic. The strengthening low appears to trigger an
285 amplification of the climatological ridge-trough-ridge pattern over North America and the
286 Atlantic, which develops 5 days prior to the event and then intensifies leading up to the
287 event.

288
289 Coincident with the anomalous upper-level cyclonic circulation, we find a region of
290 anomalous ascent in the central Pacific and weak descent in the tropical central Pacific at
291 a lag of 8 days (Fig. 2b). This alternating anomaly pattern in the central Pacific persists in

292 the days leading up to the event. Substantial meridional wind anomalies emerge at a lag
293 of 8 days extending from East Asia across the Pacific that slowly propagates
294 northeastward (Fig. 2c). This wave-like pattern of the meridional wind anomalies
295 supports the hypothesis of Rossby wave energy propagating from the western subtropical
296 Pacific to the Gulf of Alaska. These findings are consistent with studies have suggested
297 the role of the western tropical Pacific in causing the ridge off the western coast of
298 California and in triggering the extreme winter circulation pattern^{2,10,11}. The present
299 analysis shows that a coherent hemispheric-wide signature exists in the days preceding
300 the event. We show an influence of perturbations in the remote mid-to high-latitude
301 regions on a monthly timescale but the meridional wind and vertical velocity composites
302 also hint at interactions of the subtropical Pacific and the extratropics in modulating the
303 seasonal circulation on shorter timescales to cause such dipole events. Further analysis of
304 the interactions of these forcings and processes occurring on daily to monthly timescales
305 is required to establish additional causal links.

306

307 5. Quantifying long-term trends in the NAWTD

308 Primarily due to the statistically significant increasing average winter season
309 temperatures in the western domain ($p = 0.05$), the west-east temperature difference
310 between the two domains exhibits an increasing trend on a seasonal-scale. Further, there
311 is a substantial but insignificant ($p=0.15$) increasing trend in the seasonally averaged
312 fraction of land grid cells within the western domain experiencing warm extremes.
313 Though there is a small positive trend in the fraction of the eastern domain experiencing
314 cold extremes, the magnitude of the trend is small and has low significance ($p = 0.69$).

315 Despite insignificant changes in the seasonal temperature ($p = 0.75$) or fraction of area
316 exceeding the cold threshold ($p=0.69$) over the eastern domain, we find significant
317 increases in the co-occurrence of warm extremes in the west and cold extremes in the
318 east, as characterized by the daily-scale NAWTD metric (p-value for all fractional area
319 thresholds <0.01 ; Fig. 1e). The positive trend in the frequency of occurrence of these
320 events remains significant even for events of greater spatial extent, although the
321 magnitude of the trend decreases. The average intensity of these dipole events in a
322 season, calculated as the difference in area-average temperature in the western and
323 eastern domains with simultaneously occurring extreme temperatures, also show an
324 increasing trend in the historical period. The trends in the intensity of the increasingly
325 spatially extreme dipole events are similar, with only the trend for the most extreme
326 events (30% area threshold) being significant at the 5% level (Fig. 1f).

327

328 **6. Relation to trends in large-scale atmospheric circulation patterns**

329 Next, we test the hypothesis that the increased frequency of occurrence of these surface
330 dipole events is associated with a greater frequency of occurrence of the associated
331 atmospheric pattern. Using Self-Organizing Maps (SOM), we classify daily historical
332 winter atmospheric patterns over the domain (20-80°N and 150-340°E) into 20
333 representative clusters of winter weather circulations and catalogue the dipole events
334 associated with these clusters (see Methods). The choice of the domain (grey box in Fig.
335 1d) allows us to fully capture the trough-ridge-trough-ridge pattern that extends from the
336 north Pacific to the north Atlantic.

337

338 After identifying the SOMs, we use spatial pattern correlations to further identify six
339 clusters that most closely resemble the observed geopotential height composite pattern of
340 all the 15% fractional area threshold dipole events (Fig. 3). Despite the fact that these
341 clusters vary in the zonal location of the mid-latitude anomalous ridge-trough pattern and
342 the high-latitude circulation anomalies, they all have ridging over parts of the western
343 U.S. and troughing over parts of central or eastern U.S. This mid-tropospheric ridging is
344 typically associated with warmer surface conditions in the west and the troughing
345 supports the advection of cold Arctic air to the mid-latitudes, enhancing the
346 climatological surface temperature dipole between these regions. Therefore, these
347 patterns create the atmospheric configurations that support the dipole surface temperature
348 warm-west cool-east anomaly pattern. Not surprisingly, these six patterns are associated
349 with the largest number of historical dipole events (>58% collectively). Of these six
350 patterns, four patterns show an increasing trend (one is significant at the 5% level) in the
351 seasonal frequency of occurrence over time. In each season, we calculate the fraction of
352 all days associated with each cluster that have surface dipole occurrences (Fig. 3b). We
353 find that three of these clusters also show a substantial positive trend (significant at the
354 5% level) in the number of dipole events associated with them in each season. From this
355 analysis, we conclude that the increasing frequency of occurrence of the NAWTD events
356 can partly be explained by the dynamic effect of increasing frequency of occurrence of
357 the atmospheric configurations that have historically bseen associated with these events.
358

359 The relatively large trend in the fraction of dipole events (Fig. 3b) associated with each
360 cluster suggests an additional thermodynamic contribution independent of the

361 atmospheric circulation that leads to a greater occurrence of dipole events when these
362 atmospheric configurations exist. (*Will add quantification like in Horton et al. 2015*) The
363 thermodynamic effect could arise from the effect of surface warming and increased
364 occurrence of warm extremes caused by increased radiative forcing in recent decades,
365 which is consistent with the seasonal warming trend in the west and the positive trend in
366 the fraction of the west experiencing warm extremes (Fig. 1b). The eastern U.S. has not
367 warmed and in fact has a slight winter cooling over this time period with a negligible
368 increase in the fractional area experiencing cold extremes (Fig. 1a,b), contrary to the
369 enhanced surface radiative forcing effect.

370

371 **7. Likelihood in the historical and pre-industrial climates**

372 The observed trend is a consequence of both natural variability and the response to
373 external climate forcings. Are these trends attributable to anthropogenic forcings in recent
374 decades? To answer this question, we assess the contribution of natural variability and the
375 forced response to the observed positive trend. The observed trends in west and east
376 seasonal average temperature and fractional area experiencing extremes lie within the
377 range of the trends simulated in the historical LENS simulations (Fig. 4a,b). Further, the
378 forced response as represented by the historical ensemble average is able to simulate the
379 increasing trend in the seasonal average western U.S. temperature and increasing
380 fractional western U.S. area experiencing extremes but not trends in the eastern U.S.
381 temperature and the fractional region experiencing extremes. Despite that, the ensemble
382 average of the historical simulations does show an increasing frequency of dipole events
383 but simulates a weaker magnitude of the trend (Fig 4a-c). Although the ensemble average

384 shows a decreasing trend in the dipole severity measure (Fig. 4d), the observed trend is
385 positive and lies within the range of the simulated trends. Studies have demonstrated that
386 global climate models underestimate trends in Arctic Sea Ice loss^{35,36}, Eurasian Snow
387 Cover⁷, and tropical Pacific warming^{37,38}, and do not accurately capture their relevant
388 interactions^{7,39} that are requisite for simulating their impact on regional and global
389 climate. Therefore, further evaluation of the representation of the physical causal links
390 found in section 4 will be required to explain some of these model biases in the forced
391 response (as represented by the ensemble average) relative to the observations.

392

393 Applying the Kolmogorov test, we find that the distributions of 38-year trends in the
394 frequency of occurrence and intensity of dipole events in the historical and preindustrial
395 climates are not statistically distinguishable from each other (*add KS test results to Fig.*
396 *4*). For all but the 25% area events, we find that there is a slightly higher likelihood of
397 getting an increasing trend in dipole events in the historical climate than in the
398 preindustrial climate (Fig. Sx). We find the greatest difference in likelihood is for the
399 positive trend in dipole events defined on the basis of 15% of fractional domain
400 experiencing extremes. A positive trend in this measure of dipole frequency occurs in
401 approximately 53% of the control simulations and 60% of the historical simulations,
402 making it approximately 20% more likely in the historical climate than the preindustrial
403 climate (Fig. 4c). This is equivalent to saying that there is a one in two chance of a 38-
404 year period with a positive trend in dipole events in the preindustrial climate and a two in
405 three chance in the historical climate. Comparing the trends in dipole severity in the two
406 climates, we find that the median of these distributions is lower in the historical climate

407 than in the preindustrial for all dipole events, and that a positive trend in dipole severity is
408 less likely in the historical climate. Events defined with the 5%, 10% and 30% area
409 thresholds have the greatest decrease of ~20% in this likelihood in the historical climate
410 relative to the preindustrial climate opposite to the observed increasing trend. Given the
411 similarity of these trend distributions in both dipole characteristics, the small difference
412 in likelihood of dipole frequency in the two climates, and the lower likelihood of the
413 observed trend in dipole severity in the historical climate, this analysis suggests a
414 substantial role of natural variability in causing the observed trends in these events. (*Need*
415 *to include a statistical test that quantifies the probability of a positive trend*)

416

417 Despite the slight cooling trend observed over the eastern U.S. domain in recent decades,
418 we observe an increasing frequency and severity of these dipole events. Are these trends
419 likely to continue even though both these domains are projected to warm in the following
420 decades under the influence of increased radiative forcing? With the caveat that climate
421 models might not simulate the physical processes that are associated with such events, we
422 analyze future projections of such dipole events (based on the baseline percentile
423 thresholds) under the RCP 8.5 radiative forcing scenario to answer this question. To the
424 extent that we can approximate the forced response of the climate system using an
425 ensemble average of the LENS realizations, we find a non-linear response of these events
426 to increased forcing. The ensemble average of the seasonal dipole frequency shows no
427 considerable increasing or decreasing trend till the 2040's but beyond that there is a
428 significantly decreasing trend till the end of the 21st century. Similarly, we find that the
429 ensemble mean for the dipole severity also plateaus for a couple more decades and then

430 shows a monotonic decreasing trend. Throughout the 21st century, we see a monotonic
431 increase in the seasonal average temperature in the western and eastern domain. On a
432 seasonal average basis, the average fraction of the west exceeding the warm threshold
433 also increases monotonically whereas the fraction of the east below the cold threshold
434 decreases though at a slower rate with time. Even though these dipole events are defined
435 on a daily-scale, their trends are not unlikely in the context of these mean shifts in the
436 temperature distribution with warming. The number of exceedances below the cold
437 threshold is likely to decrease in the absence of a substantial change in the variability of
438 temperature and previous studies have shown that this variability is projected to decrease
439 with increased warming. Here, we note that these results do not imply anything about the
440 changes to the large-scale dynamics associated with these events that are expected to
441 occur with increasing Arctic Amplification or warming of the tropical West Pacific.
442 Further, we have not analyzed changes in the atmospheric circulations that we have
443 shown are related to these events in the historical period. In this analysis, we primarily
444 focus on the first-order effect of increased warming that will shift the distributions in a
445 direction that reduces the frequency of occurrence of these dipole events that are defined
446 based on thresholds in the baseline period. We also note that despite this effect of
447 increased global warming, there are still seasons in the mid to late 21st century that have
448 occurrences of such dipole events and the projected warming under an extreme radiative
449 forcing scenario does not completely occlude the occurrence of cold winters that we
450 experience in the current climate.

451

452 **8. Conclusions**

453

454 **References**

- 455 1. Diffenbaugh, N. S., Swain, D. L. & Touma, D. Anthropogenic warming has
456 increased drought risk in California. *Proc. Natl. Acad. Sci.* **112**, 3931–3936
457 (2015).
- 458 2. Lee, M.-Y., Hong, C.-C. & Hsu, H.-H. Compounding effects of warm sea surface
459 temperature and reduced sea ice on the extreme circulation over the extratropical
460 North Pacific and North America during the 2013–2014 boreal winter. *Geophys.*
461 *Res. Lett.* **42**, 1612–1618 (2015).
- 462 3. Swain, Daniel L, Tsiang Michael, Haugen Matz, Singh Deepti, Charland Allison,
463 Rajaratnam Bala, Diffenbaugh Noah S. 2 . THE EXTRAORDINARY
464 CALIFORNIA DROUGHT OF 2013 / 2014 : CHARACTER , CONTEXT , AND
465 THE ROLE OF CLIMATE CHANGE. *Bull. Am. Meteorol. Soc.* 3–7 (2014).
- 466 4. Cohen, J. *et al.* Recent Arctic amplification and extreme mid-latitude weather. *Nat.*
467 *Geosci* **7**, 627–637 (2014).
- 468 5. Francis, J. A. & Vavrus, S. J. Evidence linking Arctic amplification to extreme
469 weather in mid-latitudes. *Geophys. Res. Lett.* **39**, L06801 (2012).
- 470 6. Overland, J. *et al.* The Melting Arctic and Mid-latitude Weather Patterns: Are
471 They Connected? *J. Clim.* (2015). doi:10.1175/JCLI-D-14-00822.1
- 472 7. Furtado, J., Cohen, J., Butler, A., Riddle, E. & Kumar, A. Eurasian snow cover
473 variability and links to winter climate in the CMIP5 models. *Clim. Dyn.* 1–15
474 (2015). doi:10.1007/s00382-015-2494-4
- 475 8. Cohen Judah, Jones Justin, Furtado Jason C., T. E. Warm Arctic, cold continents:
476 A common pattern related to Arctic sea ice melt, snow advance, and extreme
477 winter weather. *Oceanography* **26**, 150–160 (2013).
- 478 9. Handorf, D., Jaiser, R., Dethloff, K., Rinke, A. & Cohen, J. Impacts of Arctic sea
479 ice and continental snow cover changes on atmospheric winter teleconnections.
480 *Geophys. Res. Lett.* **42**, 2367–2377 (2015).
- 481 10. Wang, S.-Y., Hipps, L., Gillies, R. R. & Yoon, J.-H. Probable causes of the
482 abnormal ridge accompanying the 2013–2014 California drought: ENSO precursor
483 and anthropogenic warming footprint. *Geophys. Res. Lett.* **41**, 3220–3226 (2014).
- 484 11. Hartmann, D. L. Pacific sea surface temperature and the winter of 2014. *Geophys.*
485 *Res. Lett.* **42**, 1894–1902 (2015).

- 486 12. Ding, Q. *et al.* Tropical forcing of the recent rapid Arctic warming in northeastern
487 Canada and Greenland. *Nature* **509**, 209–212 (2014).
- 488 13. Trenberth, K. E., Fasullo, J. T., Branstator, G. & Phillips, A. S. Seasonal aspects of
489 the recent pause in surface warming. *Nat. Clim. Chang.* **4**, 911–916 (2014).
- 490 14. Wang, S.-Y. S., Huang, W.-R. & Yoon, J.-H. The North American winter ‘dipole’
491 and extremes activity: a CMIP5 assessment. *Atmos. Sci. Lett.* n/a–n/a (2015).
492 doi:10.1002/asl2.565
- 493 15. Screen, J. A. & Simmonds, I. Increasing fall-winter energy loss from the Arctic
494 Ocean and its role in Arctic temperature amplification. *Geophys. Res. Lett.* **37**,
495 n/a–n/a (2010).
- 496 16. Kim, B.-M. *et al.* Weakening of the stratospheric polar vortex by Arctic sea-ice
497 loss. *Nat Commun* **5**, (2014).
- 498 17. Cohen, J., Furtado, J. C., Barlow, M., Alexeev, V. A. & Cherry, J. E. Arctic
499 warming, increasing snow cover and widespread boreal winter cooling. *Environ.*
500 *Res. Lett.* **7**, 14007 (2012).
- 501 18. Jaiser, R., Dethloff, K., Handorf, D., Rinke, A. & Cohen, J. Impact of sea ice cover
502 changes on the Northern Hemisphere atmospheric winter circulation. *Tellus A; Vol*
503 *64* (2012). at <<http://www.tellusa.net/index.php/tellusa/article/view/11595>>
- 504 19. Screen, J. A. & Simmonds, I. Amplified mid-latitude planetary waves favour
505 particular regional weather extremes. *Nat. Clim. Chang.* **4**, 704–709 (2014).
- 506 20. Cohen, J., Barlow, M., Kushner, P. J. & Saito, K. Stratosphere–Troposphere
507 Coupling and Links with Eurasian Land Surface Variability. *J. Clim.* **20**, 5335–
508 5343 (2007).
- 509 21. Overland, J. E., Wood, K. R. & Wang, M. Warm Arctic-cold continents: Climate
510 impacts of the newly open arctic sea. *Polar Res.* **30**, (2011).
- 511 22. Petoukhov, V. & Semenov, V. A. A link between reduced Barents-Kara sea ice
512 and cold winter extremes over northern continents. *J. Geophys. Res. Atmos.* **115**,
513 n/a–n/a (2010).
- 514 23. Tang, Q., Zhang, X., Yang, X. & Francis, J. a. Cold winter extremes in northern
515 continents linked to Arctic sea ice loss. *Environ. Res. Lett.* **8**, 014036 (2013).
- 516 24. Kay, J. E. *et al.* The Community Earth System Model (CESM) Large Ensemble
517 Project: A Community Resource for Studying Climate Change in the Presence of
518 Internal Climate Variability. *Bull. Am. Meteorol. Soc.* (2014). doi:10.1175/BAMS-
519 D-13-00255.1

- 520 25. Kohonen, T. *Self-Organizing Maps*. Springer Series in Information Sciences **30**,
521 (Springer , 2001).
- 522 26. Johnson, N. C. How Many ENSO Flavors Can We Distinguish?*. *J. Clim.* **26**,
523 4816–4827 (2013).
- 524 27. Horton, D. E. *et al.* Contribution of changes in atmospheric circulation patterns to
525 extreme temperature trends. *Nature* **522**, 465–469 (2015).
- 526 28. Singh, D. *et al.* 2013 Severe Flooding in Northern India in June 2013: Quantifying
527 the likelihood of extreme June precipitation in the current and pre-industrial
528 climates. “*Explaining Extrem. Events 2013 from a Clim. Perspect. Bull. Am.*
529 *Meteorol. Soc.* **95**, S58–61 (2014).
- 530 29. Dawson, A. & Palmer, T. N. Simulating weather regimes: impact of model
531 resolution and stochastic parameterization. *Clim. Dyn.* **44**, 2177–2193 (2015).
- 532 30. Bao, M. & Wallace, J. M. Cluster Analysis of Northern Hemisphere Wintertime
533 500-hPa Flow Regimes 1920–2014. *J. Atmos. Sci.* (2015). doi:10.1175/JAS-D-15-
534 0001.1
- 535 31. Skific, N., Francis, J. A. & Cassano, J. J. Attribution of Projected Changes in
536 Atmospheric Moisture Transport in the Arctic: A Self-Organizing Map
537 Perspective. *J. Clim.* **22**, 4135–4153 (2009).
- 538 32. Cattiaux, J., Douville, H. & Peings, Y. European temperatures in CMIP5: origins
539 of present-day biases and future uncertainties. *Clim. Dyn.* **41**, 2889–2907 (2013).
- 540 33. Driouech, F., Déqué, M. & Sánchez-Gómez, E. Weather regimes—Moroccan
541 precipitation link in a regional climate change simulation. *Glob. Planet. Change*
542 **72**, 1–10 (2010).
- 543 34. Cassano, J. J., Uotila, P., Lynch, A. H. & Cassano, E. N. Predicted changes in
544 synoptic forcing of net precipitation in large Arctic river basins during the 21st
545 century. *J. Geophys. Res. Biogeosciences* **112**, n/a–n/a (2007).
- 546 35. Swart, N. C., Fyfe, J. C., Hawkins, E., Kay, J. E. & Jahn, A. Influence of internal
547 variability on Arctic sea-ice trends. *Nat. Clim. Chang.* **5**, 86–89 (2015).
- 548 36. Stroeve, J. C. *et al.* Trends in Arctic sea ice extent from CMIP5, CMIP3 and
549 observations. *Geophys. Res. Lett.* **39**, n/a–n/a (2012).
- 550 37. Meehl, G. A., Teng, H. & Arblaster, J. M. Climate model simulations of the
551 observed early-2000s hiatus of global warming. *Nat. Clim. Chang.* **4**, 898–902
552 (2014).

553 38. Kosaka, Y. & Xie, S.-P. Recent global-warming hiatus tied to equatorial Pacific
554 surface cooling. *Nature* **501**, 403–407 (2013).

555 39. Trenberth, K. E., Fasullo, J. T. & Shepherd, T. G. Attribution of climate extreme
556 events. *Nat. Clim. Chang. advance on*, (2015).

557

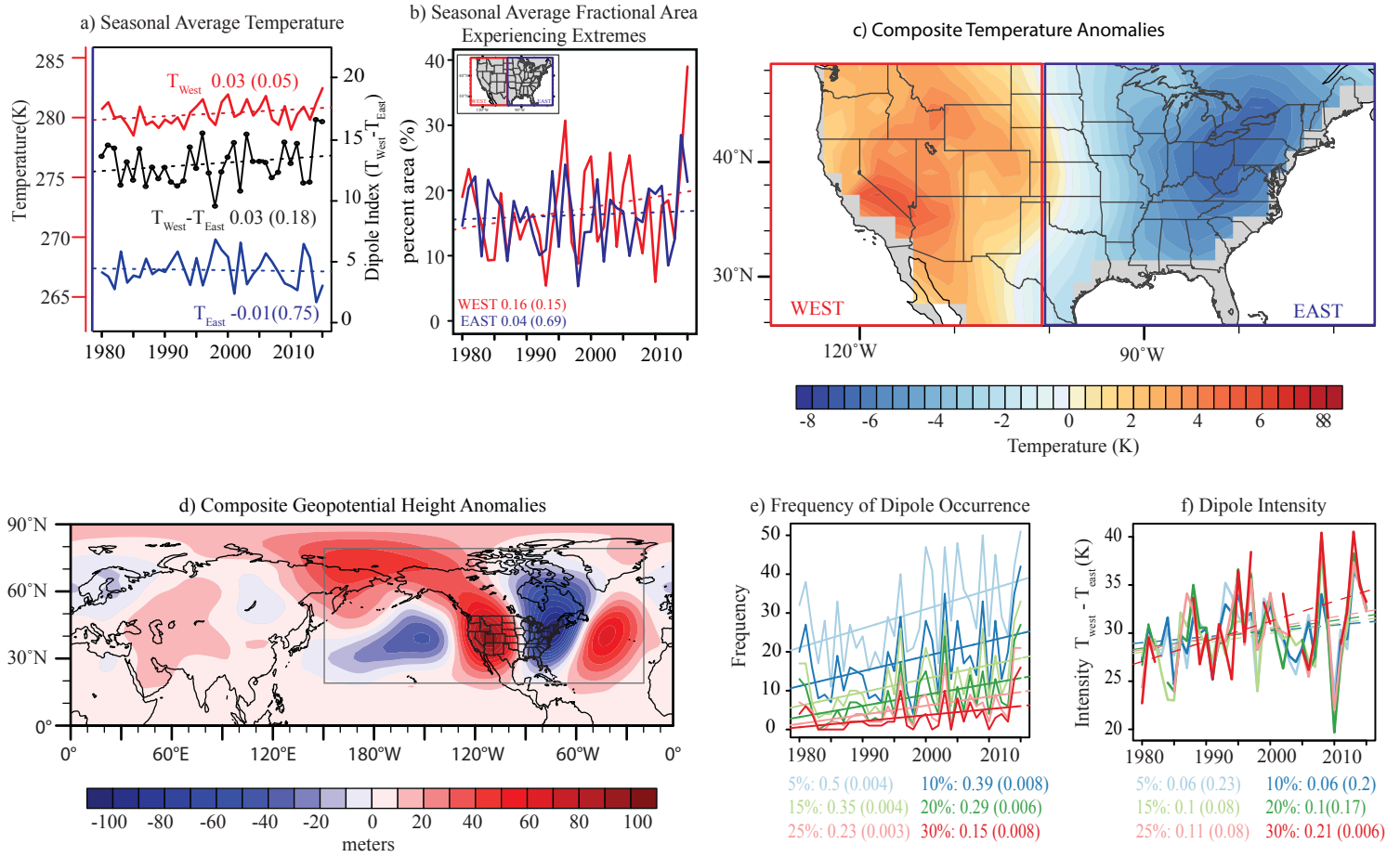


Figure 1. North American Winter Temperature Dipole (NAWTD): (a) Timeseries of seasonal average daily maximum temperature of the western U.S. (red) and daily minimum temperature in the eastern U.S. (blue) (refer to left y-axis), and their temperature difference (black; refer to right y-axis). (b) Average fraction of the land in the west exceeding the hot threshold (red) and east below the cold threshold (blue). (c) Near-Surface (2m) temperature anomaly composite and (d) mid-tropospheric (500mb) geopotential height anomaly composite of all historical dipole events (1980-2015); grey box encloses the domain with substantial geopotential height anomalies. Dipole events are defined as days with daily maximum temperature over at least 15% of the land domain in the west exceeding the 85th percentile threshold concurrent with daily minimum temperature in the east falling below the 15th percentile threshold at each grid point (referred to as 15% area dipole events). (e) Number of occurrences of dipole events in a season based on different thresholds for the respective land fractions concurrently exceeding the hot and cold thresholds. (f) Average intensity of dipole events in a seaons, defined as the difference in the spatially averaged temperature of the west and east domains exceeding the thresholds; colors in (e) and (f) represent the different minimum fractional area thresholds used to define the dipole events.

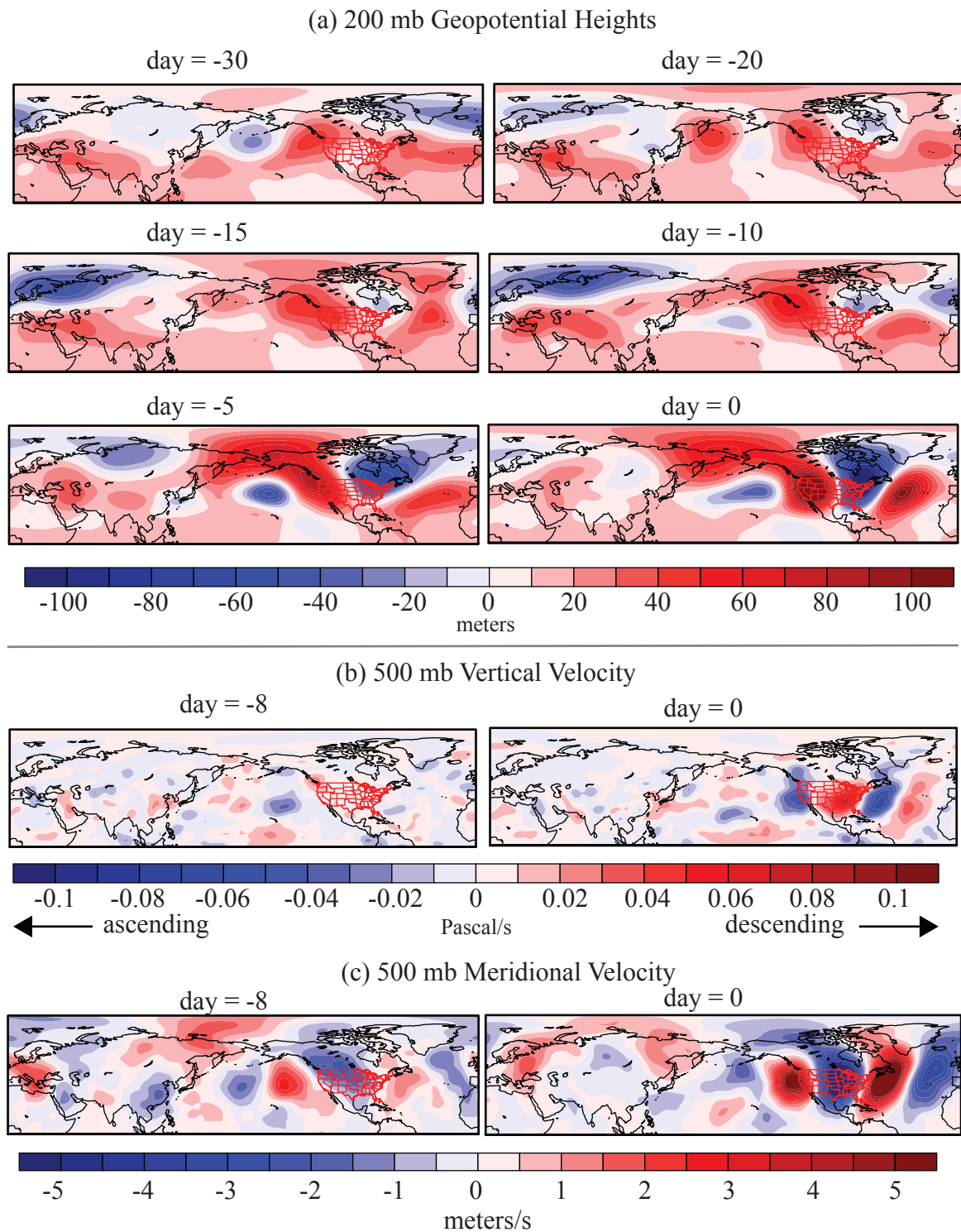


Figure 2. Remote Connections: Lagged composites of (a) jet-level (200mb) geopotential heights, (b) 500mb vertical velocity (ω) and (c) 500mb meridional velocity for all 15% area threshold dipole events. Composites of geopotential height start at 30 days prior to the event. Vertical velocity and meridional wind composites are only shown for the day of the event and for a lag of 8 days. Refer to supplement for composites at other lags.

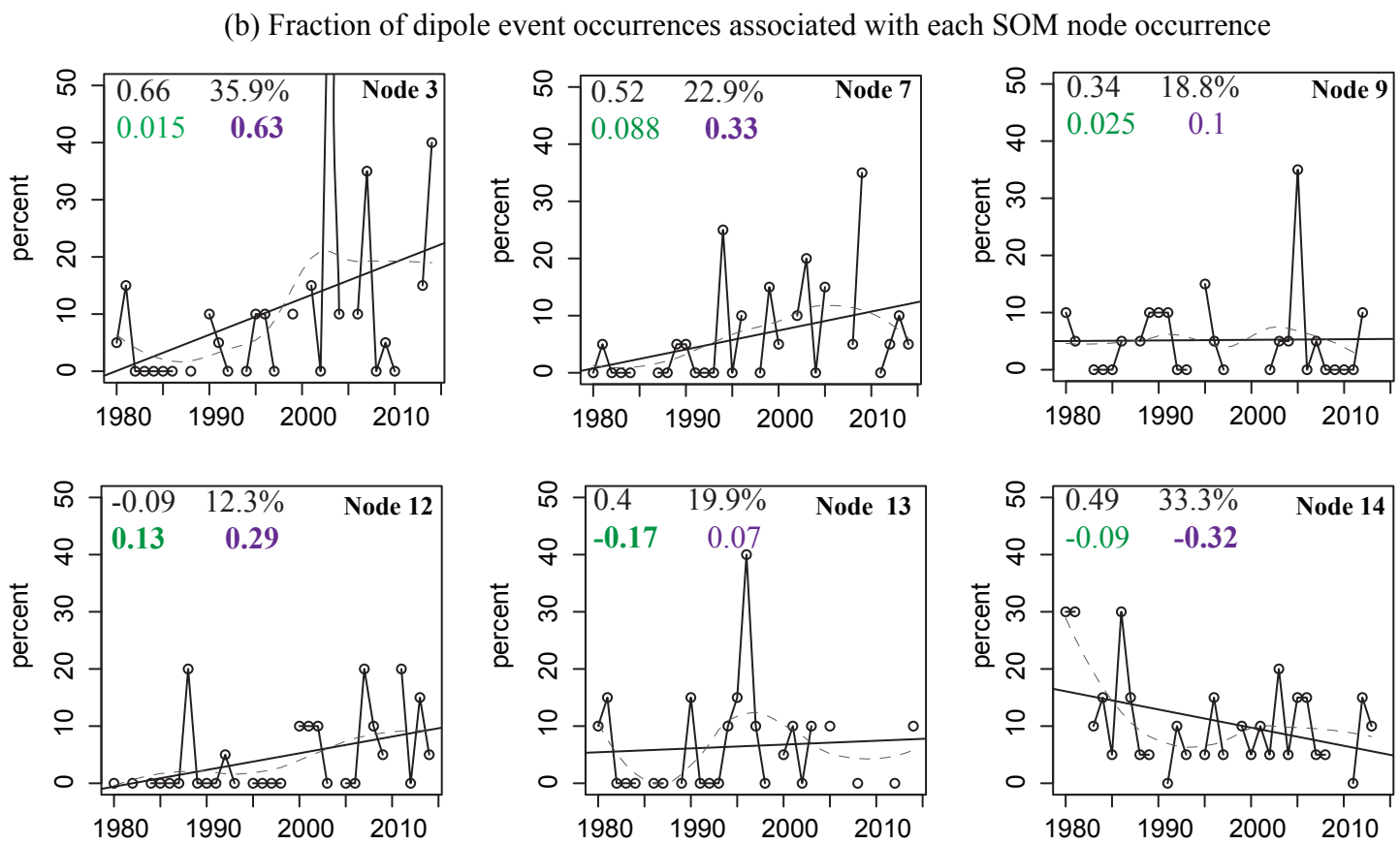
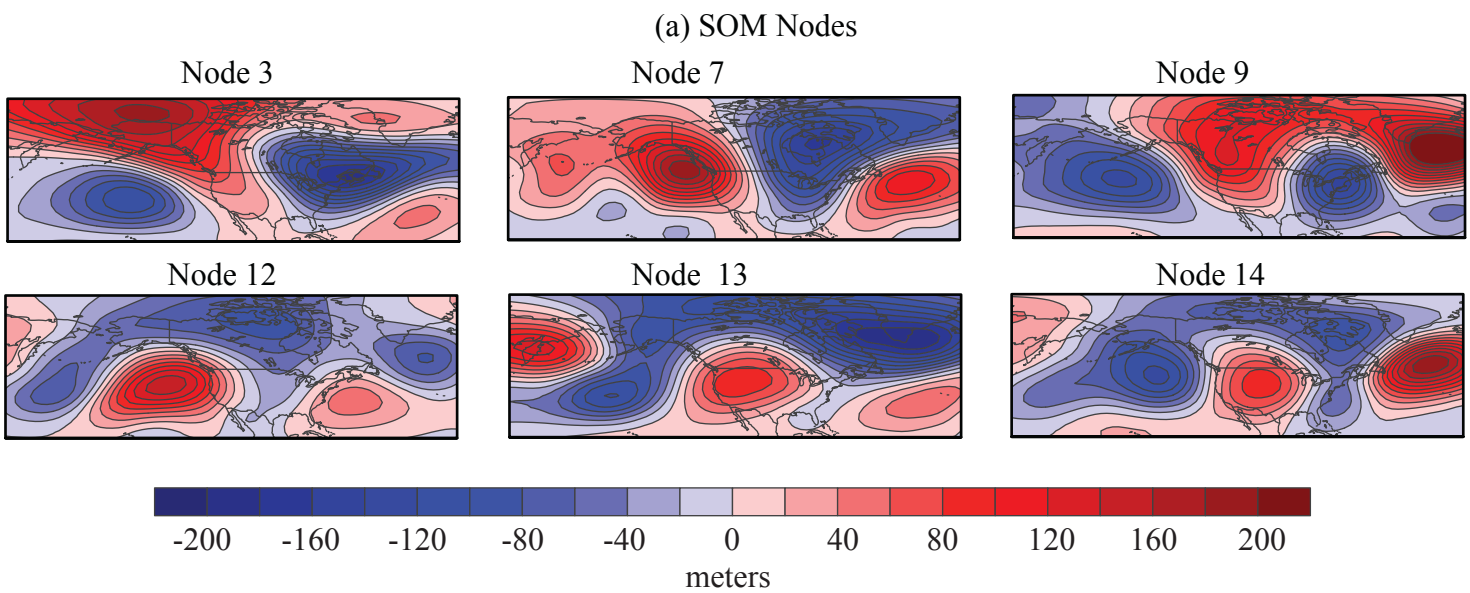


Figure 3. Associated Circulation Trends: (a) Six of twenty SOM nodes derived from 500mb mid-tropospheric geopotential height anomalies. These six nodes account for the largest fraction of 15% area threshold dipole events. (b) Trends in the fraction of SOM node occurrences that are dipole events; numbers indicate the correlation of the 500mb composite for these dipole events with the SOM node (top left), fraction of SOM occurrence that are dipole events (top right), trend in the SOM circulation pattern occurrence (bottom left; green) and trend in the fraction of SOM occurrence that are dipole events (bottom right; purple).

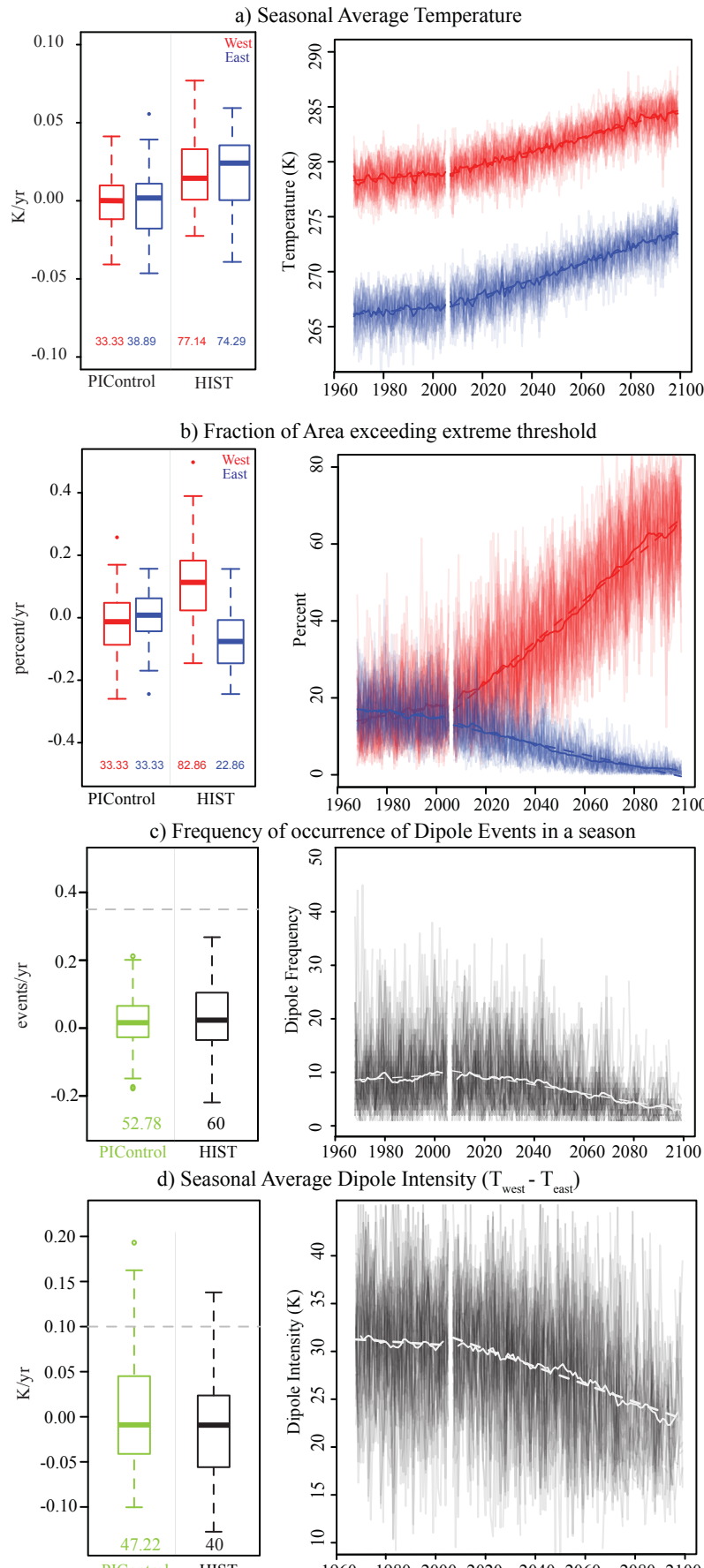


Figure 4. Trend Attribution: (left panels) Distribution of 38 year trends in (a) seasonal average temperatures over the west and east domains, (b) seasonal average fraction of the land in the west exceeding the grid-point hot threshold and in the east falling below the grid-point cold threshold, (c) frequency of occurrence of 15% fractional area threshold dipole events, (d) average intensity of dipole events in a season, from the pre-industrial (PIControl) and historical (HIST) LENS simulations. (right panels) Time series of these variables from all 35 realizations in the historical and RCP8.5 future climate scenario. The straight lines indicates the linear trend in the ensemble averageand the curve shows a 5-year moving average.